GAS TURBINE ROTOR/CASE STRUCTURAL RESPONSE TO ROTATING STALL:

EXPERIMENTAL DOCUMENTATION AND ANALYTICAL APPROACH*

Philip J. Haley
Detroit Diesel Allison
Division of General Motors Corp.
Indianapolis, Indiana 46206

SUMMARY

This work presents experimental data describing the forcing functions and structural responses characterizing gas turbine rotor/case system vibration due to rotating stall in an axial-flow compressor. Two data sets with fundamentally different response characteristics are presented; one is supersynchronous and the other subsynchronous. Conventional beam-element rotor dynamics analysis is shown to be severely limited in its ability to predict these responses. A new analytical approach, which significantly increases structural response predictive capability for these phenomena, is briefly discussed.

INTRODUCTION AND BACKGROUND

The emphasis on aerothermodynamic performance in the high-performance gas turbine engine of today and tomorrow has focused attention on increased performances from its components, one of which is the axial-flow compressor. Compressor design trends, aimed toward high efficiencies and/ or high aerodynamic loadings, have led to machines that are very sensitive to running tip clearances between blades/vanes and their respective case/ rotor structures. The controlling criterion in the selection of these clearances is often the necessity to accommodate rotor and case excursions associated with surge/stall instabilities. Closely related to clearance selection is the rotor dynamic design of a given machine. The mechanical designer typically has only empirical guidelines based on severely limited data with which to design to accommodate surge/stall deflections and to simultaneously provide minimum running clearances. This paucity of knowledge of structural dynamic response during surge/stall instabilities renders the optimization of tip clearances, rotor/ case flexibility, and bearing placement a difficult and abstract task.

Detroit Diesel Allison (DDA) is currently working under Air Force contract to experimentally document compressor structural response to the rotating stall phenomenon and to improve state-of-the-art analytical techniques for predicting such response. These efforts address some of the deficiencies in knowledge noted above. This paper presents an abbreviation of some of the results of this contractual effort with emphasis on the experimental data.

Rotating stall can be viewed as one or more regions or "cells" of low momentum, low-pressure fluid, each covering some sector of the flow annulus of the compressor. Although rotating stall typically occurs near the compressor surge line, some machines exhibit it away from surge, even near the operating line. The number of cells can vary from one to eight or more. Multiple cells seem to be uniformly spaced circumferentially. In the fully developed rotating stall considered herein, the cells traverse the axial length of the com-

---

pressor, so can be regarded as "tubes" of low-pressure fluid that are axially twisted or "corkscrewed" through the machine. These stall cells result in net forces exerted on both the compressor rotor and the case, assuming the cell fills the flow passage span. These forces are radial and, if ramp angles are present, can have axial components. The stall pattern rotates in the direction of the compressor rotor but at partial rotor speed, generally between 25% and 75% speed, as viewed from the inertial frame. Thus a single-cell rotating stall at 50% rotor speed acts as a subsynchronous excitation mechanism. A two-cell stall at 50% speed appears as a synchronous force, while a two-cell stall at 60% speed appears supersynchronous.

In contrast to the surge phenomenon, rotating stall can produce quasi-steady, periodic forcing functions which can cause steady-state, periodic rotor/case response manifested as structural dynamic instabilities. Such responses can, based on experience, lead to high amplitude vibration and/or radial excursions beyond the design clearances, causing rub and potential structural failures. This paper presents a classic set of experimental data describing the violent nature of rotating stall-induced rotor/case system vibration. The associated forcing functions are also presented, and Fourier analysis is utilized to gain insight into the forcing function/response relationships. The new analytical approach developed at DDA to calculate stall-induced system response is briefly outlined.

EXPERIMENTAL DATA AND DISCUSSION

The data presented herein were generated at DDA on a large, multistage, axial-flow compressor rig, which is fairly typical of the compressors currently found in high-performance, aircraft-type gas turbines. This rig is sketched in Figure 1. Though not shown in this sketch, the bearing/rotor arrangement of the rig is similar to that of the parent gas generator, of which this compressor is a component. This rig was instrumented to measure the time-variant forcing functions and structural responses associated with rotating stall. The elements of this high-response instrumentation scheme are shown in Figure 2, which depicts the compressor case unwrapped into a plane. These sensors are all mounted on the compressor case in the stationary frame. The dynamic pressure sensors are high-response transducers flush-mounted in the outer gas-path wall. They measure the fluctuating component of endwall pressure, which is assumed to characterize the stall cell at both its inner and outer span. Vibration pickups measure case velocities, while rotor-to-case relative motion is sensed with "whip" pickups, which are proximity probes located over compressor blade tips. Rotor motion can be established by vectorially adding case motion and rotor-to-case relative motion after transforming these measured parameters to compatible units.

Running of this compressor rig produced several rotating stall and/or surge sequences, which were recorded on magnetic tape via the described instrumentation. The phenomenological sequence from which the data presented herein were quantified consists of a high-speed surge followed by two-zone and then single-zone rotating stall patterns. Figure 3 is a time record of the rotor speed excursion showing the onset of surge and the subsequent initiation of the stall patterns. As seen in this figure, the entire sequence of time-variant phenomena lasted approximately 5 seconds, during which time the rotor accumulated over 900 revolutions under the influence of the related rotating forces. The data presented in the subsequent discussion were defined over the two time intervals shown in Figure 3.

Following surge, a two-zone rotating stall pattern was spontaneously established, traveling (one-per-circumference spatial propagation rate) at 57% rotor speed. Time traces of the dynamic signals over the defined analysis interval are presented in Figures 4, 5, and 6. A common timing signal on these plots is used to time-relate events. The responses shown in Figures 5 and 6 show high-amplitude compressor case structural vibration at the frequency of the individual stall cell passage from Figure 4, i.e. at two times the two-zone rotating stall rotational frequency. The whip signals of Figure 6 also indicate rotor-to-case relative motion at the same frequency. These responses and the associated forcing functions thus appear to be supersynchronous.

The two-zone rotating stall pattern evolved into a single-zone pattern (Figure 3) with a propagation rate of 60% rotor speed. Figures 7, 8, and 9 present the traces of dynamic pressure, case vibration, and whip for this stall occurrence. Again, high amplitude structural response is observed. Both the compressor case response and the whip signals visually indicate major components at the subsynchronous passing frequency of the Figure 7 forcing functions. Clearly evident in some of the response signals are additional higher frequency components.

Insight into the nature and relationships of the forcing functions and structural responses characterizing these stall phenomena is afforded by Fourier analysis. The two-zone stall data of Figures 4 through 6 were digitized over the common interval shown on Figure 4, and the single-zone data of Figures 7 through 9 were likewise digitized over the period shown on Figure 7. Digitized data were harmonically analyzed to produce components for each signal according to the cosine Fourier form:

$$\sum_{m=0}^{\infty} U_m \cos (m\Omega t - m\theta + a_m)$$

where:

U_m = amplitude of mth harmonic (harmonic coefficient)
m = harmonic index
Ω = fundamental frequency
θ = circumferential location of sensor
a_m = phase of mth harmonic
t = time

This procedure removes phase differences arising from the different circumferential locations of the various sensors. Note that in Figures 4 through 9, representing fully developed stall patterns, all these dynamic signals, considered to represent transient phenomena in the sense of an operating steady-state turbomachine, are relatively periodic functions.

The Fourier content of the pressure traces is presented in Tables I and II for the two-zone and one-zone phenomena, respectively. Because eight one-per-circumference spatial cycles were digitized (Figures 4 and 7), the first five spatial harmonics of the waveforms correspond analytically to temporal harmonics 8, 16, 24, 32, and 40, as listed. A comparison of Table I with Figure 4 for two-zone stall confirms the predominance of second harmonic content (first

harmonic of a single stall cell times two cells per circumference) and indicates a strong fourth harmonic. Comparison of Table II with Figure 7 for one-zone stall shows a predominant first harmonic content with significant higher harmonic content, notably second harmonic.

Table III presents the Fourier content of the measured responses to the two-zone rotating stall pattern. The first five spatial harmonics are listed. The amplitude predominance of second harmonic is seen, followed by fourth (first harmonic of second). This pattern corresponds to that noted in the pressure traces. The highest amplitude forcing functions (pressures) from Table I are seen to be axially toward the rear of the compressor, whereas the highest amplitude case responses from Table III are seen to be in the compressor inlet area, suggesting a proximity to a resonance in the inlet. Comparison of these two tables does clearly show, however, direct structural response to rotating stall. The presence and predominance of second and higher harmonic case response show the importance of localized distortion and "egging" behavior in a flexible gas turbine case. Beam-like behavior, corresponding to first harmonic force and response components, is a relatively minor contributor to case response in these data. Figure 10 further clarifies these descriptions.

Table IV presents the Fourier content of the measured responses to single-zone stall. The amplitude predominance of first harmonic is apparent, along with a strong second harmonic contribution, especially in the inlet. This same pattern is seen in the rotor-to-case whip signal. The relative Fourier contents of these response signals are comparable to those of the forcing functions (Table II), again suggesting the approach of comparing forces and responses on a harmonic basis. These data indicate the primary case response to be beam-like, unlike that observed in the two-zone phenomenon.

As shown in Figure 2, axially-redundant signals were obtained for several parameters. Examination of the Fourier content of these signals in Tables III and IV reveals circumferentially asymmetric responses throughout this compressor in both first and second harmonic components for both case and rotor-to-case signals. The significance of these observations is that the responses of this "axisymmetric" turbomachine to these stall-induced forcing functions are not at all axisymmetric. The asymmetric case response in the first harmonic indicates asymmetric mounting of the case to ground for the beam-like motion. Asymmetric case response in the second and higher harmonics is due to asymmetry in the case itself, caused by holes, split lines, bleed manifolds, and other deviations from pure axisymmetry.

A conclusion from these experimental data is that stall-induced response of the compressor case, an important contributor to system dynamic response and to rotor-to-case clearance response, cannot always be adequately described by first harmonic, beam-like motion. Furthermore, significant circumferential asymmetry is present in the different modes of case response. Obvious from these observations is the fact that the beam-element analytical approach widely used in rotor dynamic analyses is generally inadequate for modeling either of the forced response problems described herein. Since the supersynchronous two-zone stall is seen to have only minor components of forcing functions and responses that can be described by the first spatial harmonic, the beam-element approach is inherently grossly inadequate. Although forcing functions and responses of the subsynchronous single-zone stall have predominant first harmonic content, the higher harmonic components are not negligible but are ignored in beam-element analysis.

402

NEW ANALYTICAL APPROACH

DDA has developed a capability for predicting rotor/case structural response to dynamic forcing functions. This analysis has been developed specifically for the rotating stall phenomenon in compressors. The analysis includes the ability to predict localized motions of the static structure (i.e., compressor case), including "egging" modes. The approach entails using a beam-element rotor analysis along with an axisymmetric finite-element case analysis. Egging and localized motions are calculated for the case alone and are assumed to be decoupled from the rotor. Beam-like motion is calculated for the coupled rotor/case system using finite-element case modes modally coupled to the conventional beam-element rotor model. Deviations from pure axisymmetry are recognized: (1) in the beam-element calculation, through allowance for asymmetric support modeling, and (2) in the finite-element case analysis, through availability of a discontinuous element for modeling struts, vanes, holes in the case, bleed manifolds, and other variances from pure axisymmetry. This technique has substantially addressed the shortcomings of conventional beam-element rotor dynamics analysis in the modeling of stall-induced response and has produced reasonable analytical simulations of both the subsynchronous and supersynchronous preceding experimental data sets.

TABLE I. - FOURIER DECOMPOSITON OF DYNAMIC PRESSURES FROM TWO-ZONE STALL

	Stage								
	1	2	3	5	6	7	8	9	10
Temporal harmonic = 8									
Amplitude	0.2143	0.0346	0.0613	0.0670	0.0562	0.0475	0.1012	0.0924	0.2463
Phase	-103.1	-75.9	97.0	-144.7	135.5	-149.5	-174.5	60.7	77.7
Temporal harmonic = 16									
Amplitude	0.1050	0.1597	0.1961	0.9671	1.784	2.711	2.622	3.878	2.340
Phase	-1.5	-122.6	78.1	-160.2	-176.8	-175.6	159.5	136.4	106.1
Temporal harmonic = 24									
Amplitude	0.0498	0.0334	0.0260	0.0513	0.0620	0.0561	0.0688	0.0974	0.1809
Phase	47.3	18.4	115.3	-74.0	140.6	153.8	166.4	88.4	61.6
Temporal harmonic = 32									
Amplitude	0.1022	0.1339	0.1023	0.1286	0.3121	0.5181	0.4338	0.8993	0.1992
Phase	-22.9	-24.8	-28.0	-164.8	-171.1	-154.2	141.5	102.6	117.0
Temporal harmonic = 40									
Amplitude	0.0380	0.0026	0.0001	0.0311	0.0495	0.0188	0.0526	0.0914	0.0211
Phase	0.0	-180.0	-180.0	0.0	-180.0	0.0	0.0	0.0	0.0

Amplitude in psi.
Phase in degrees.

TABLE II. - FOURIER DECOMPOSITION OF DYNAMIC PRESSURES FROM SINGLE-ZONE STALL

	Stage								
	1	2	3	5	6	7	8	9	10
Temporal harmonic = 8									
Amplitude	0.2323	0.2519	0.3808	1.041	1.576	2.222	2.122	2.139	0.7372
Phase	17.3	149.3	176.0	-157.3	-172.7	-173.5	177.1	155.6	128.1
Temporal harmonic = 16									
Amplitude	0.1429	0.0926	0.1158	0.4098	0.7246	1.111	0.9731	0.9519	0.4192
Phase	-7.6	38.3	-108.3	-134.4	-147.7	-155.3	179.7	166.4	108.8
Temporal harmonic = 24									
Amplitude	0.1128	0.0888	0.1165	0.1704	0.3000	0.4062	0.3069	0.2796	0.0043
Phase	-26.2	7.0	-47.2	-146.3	-145.2	-150.8	-164.6	-127.8	169.1
Temporal harmonic = 32									
Amplitude	0.0399	0.0845	0.0883	0.0797	0.1446	0.1212	0.0718	0.1437	0.1235
Phase	-32.8	32.1	-32.6	-124.5	-143.3	176.6	-40.8	-30.1	127.2
Temporal harmonic = 40									
Amplitude	0.0085	0.0129	0.0245	0.0408	0.0491	0.0655	0.0659	0.1723	0.0220
Phase	0.0	0.0	0.0	-180.0	-180.0	-180.0	0.0	0.0	0.0

Amplitude in psi.
Phase in degrees.

TABLE III. – FOURIER COMPONENTS OF EXPERIMENTAL RESPONSE FOR TWO-ZONE ROTATING STALL

Ref. Figures 5 & 6

Signal	Description	U_1	α_1	U_2	α_2	U_3	α_3	U_4	α_4	U_5	α_5
Vibration	Inlet hsg., 0°	0.0441	26	2.286	-28	0.1124	-226	0.1953	-170	0.0276	0
Vibration	Inlet hsg., 270°	0.0706	-174	2.499	-182	0.0835	18	0.1082	-178	0.0165	0
Vibration	Stg. 7 vane, 220°	0.0265	-200	0.6071	-269	0.0141	-105	0.0635	-243	0.0118	-180
Vibration	Stg. 8 vane, 150°	0.0453	-187	0.2829	17	0.0471	-240	0.0682	-137	0.0206	0
Vibration	Stg. 9 vane, 173°	0.0448	-231	0.7128	74	0.0060	-141	0.0275	2	0.0006	-179
Vibration	Stg. 9 vane, 355°	0.0118	2	0.6265	63	0.0129	-111	0.0171	-45	0.0035	-180
Vibration	Rear comp., 0°	0.0447	6	0.5282	68	0.0171	16	0.0329	-193	0.0129	0
Vibration	Rear comp., 150°	0.0241	-191	0.2541	-4	0.0065	49	0.0441	-268	0.0094	-180
Vibration	Rear comp., 240°	0.0271	-148	0.8876	-209	0.0218	72	0.1112	-96	0.0094	-180
Vibration	Rear comp., 270°	0.0276	-63	0.4035	-108	0.0100	22	0.0429	62	0.0035	-180
Whip	Stg. 9, 240°	0.0014	148	0.0023	201	0.0006	113	0.0002	88	0.0002	-180
Whip	Stg. 9, 150°	0.0007	77	0.0018	46	0.0006	225	0.0011	191	0.0003	0

U_m = amplitude (harmonic coefficient); vibration in in./sec., avg; whip in in., single amplitude.
α_m = phase angle, in degrees.
m = harmonic index.

TABLE IV. – FOURIER COMPONENTS OF EXPERIMENTAL RESPONSE FOR SINGLE-ZONE ROTATING STALL

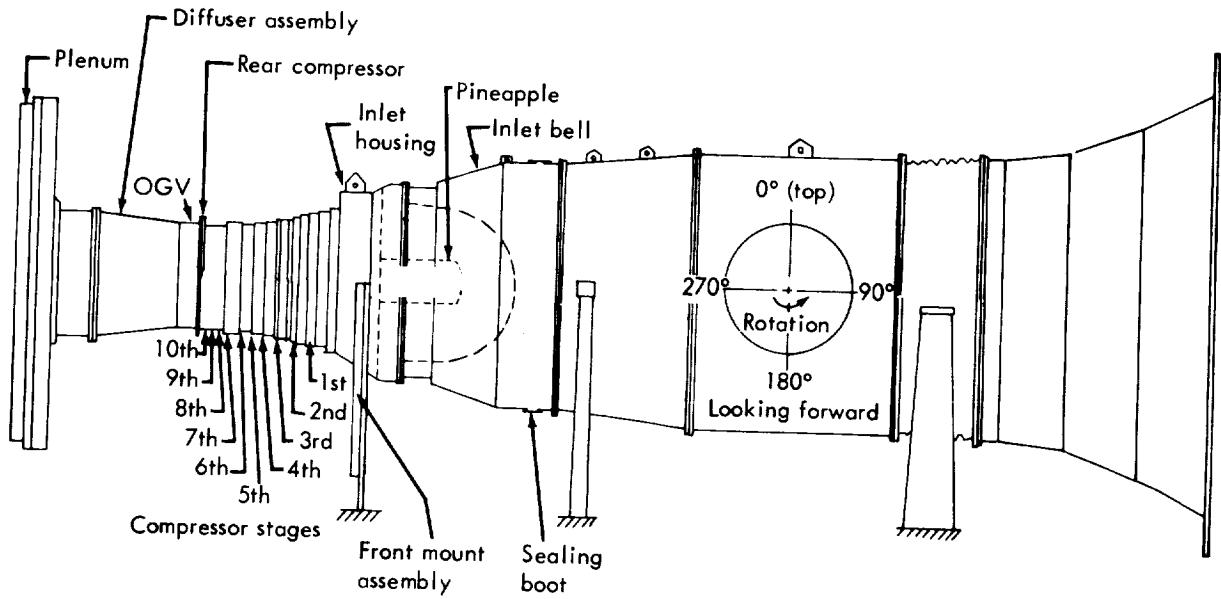Ref. Figures 8 & 9

Signal	Description	U_1	α_1	U_2	α_2	U_3	α_3	U_4	α_4	U_5	α_5
Vibration	Inlet hsg., 0°	1.059	63	0.9482	45	0.0553	-257	0.0676	-62	0.0276	0
Vibration	Inlet hsg., 270°	0.6907	-41	0.9385	-133	0.1021	75	0.0388	-58	0.0137	-180
Vibration	Stg. 7 vane, 220°	0.8600	-77	0.3906	-221	0.2041	-150	0.0512	-200	0.0165	0
Vibration	Stg. 8 vane, 150°	0.6681	-104	0.3110	25	0.0269	-182	0.0525	-14	0.0006	-179
Vibration	Stg. 9 vane, 173°	1.038	-107	0.2897	80	0.1545	-181	0.0333	-19	0.0200	0
Vibration	Stg. 9 vane, 355°	0.9588	66	0.4257	-232	0.1152	-89	0.0281	-43	0.0072	-180
Vibration	Rear comp., 0°	0.9194	40	0.3806	-240	0.0576	-110	0.0194	-28	0.0109	-180
Vibration	Rear comp., 150°	0.6627	-135	0.2436	-5	0.0579	-184	0.0657	-44	0.0161	-180
Vibration	Rear comp., 240°	1.485	-88	0.3059	-133	0.0376	-108	0.1682	-225	0.0171	-180
Vibration	Rear comp., 270°	0.5379	-30	0.2448	-48	0.1325	-23	0.0287	-107	0.0096	-180
Whip	Stg. 9, 240°	0.0112	-36	0.0029	-70	0.0011	-100	0.0005	244	0.0001	-180
Whip	Stg. 9, 150°	0.0164	-157	0.0016	61	0.0003	137	0.0006	59	0.0003	0

U_m = amplitude (harmonic coefficient); vibration in in./sec., avg; whip in in., single amplitude.
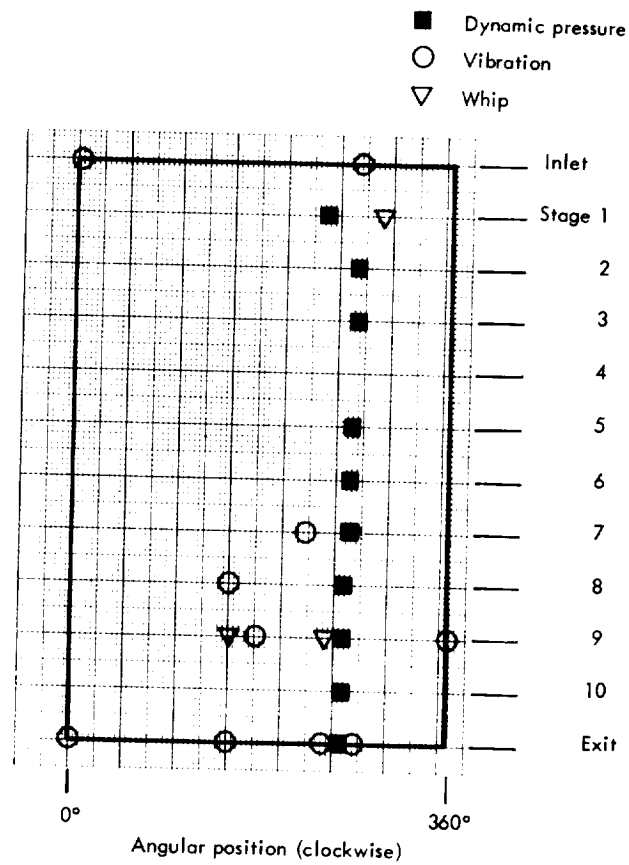α_m = phase angle, in degrees.
m = harmonic index.

Figure 1. - Compressor rig on test stand.

TE-6657

Figure 2. - High-response instrumentation scheme.
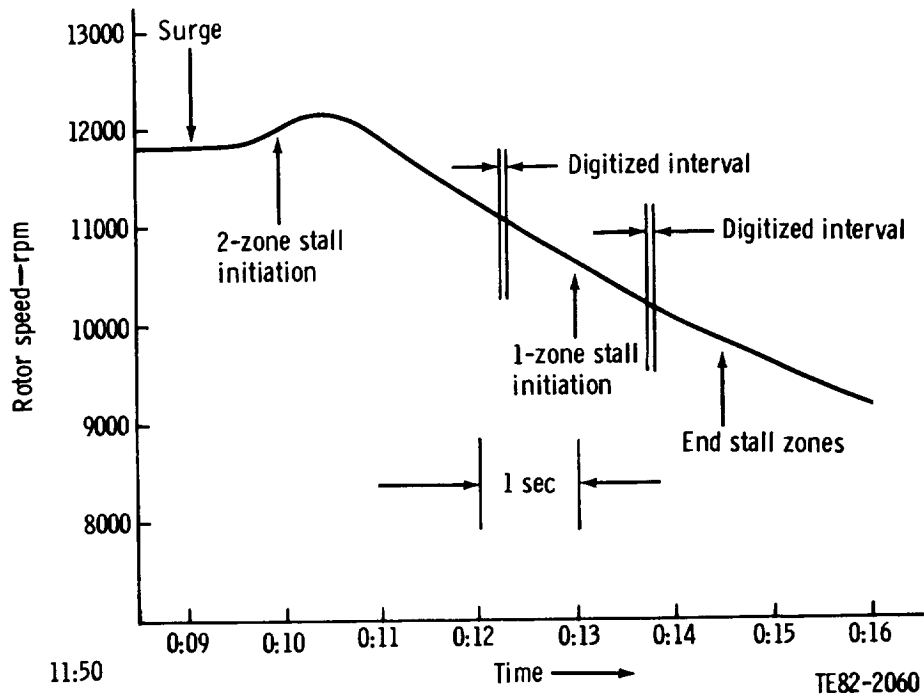
UNCLASSIFIED
TE-6714

406
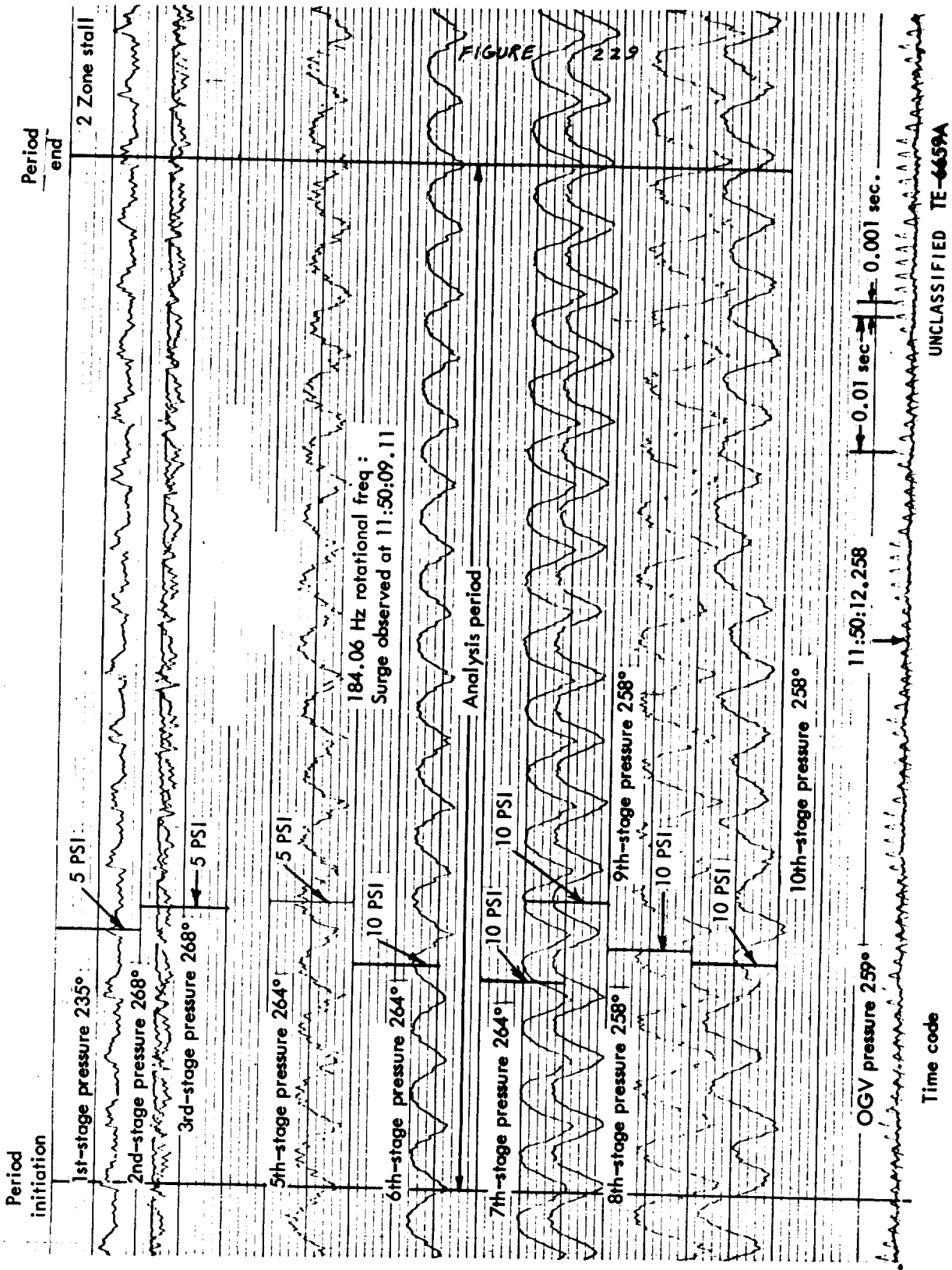
Figure 3. - Sequence of phenomena following surge.

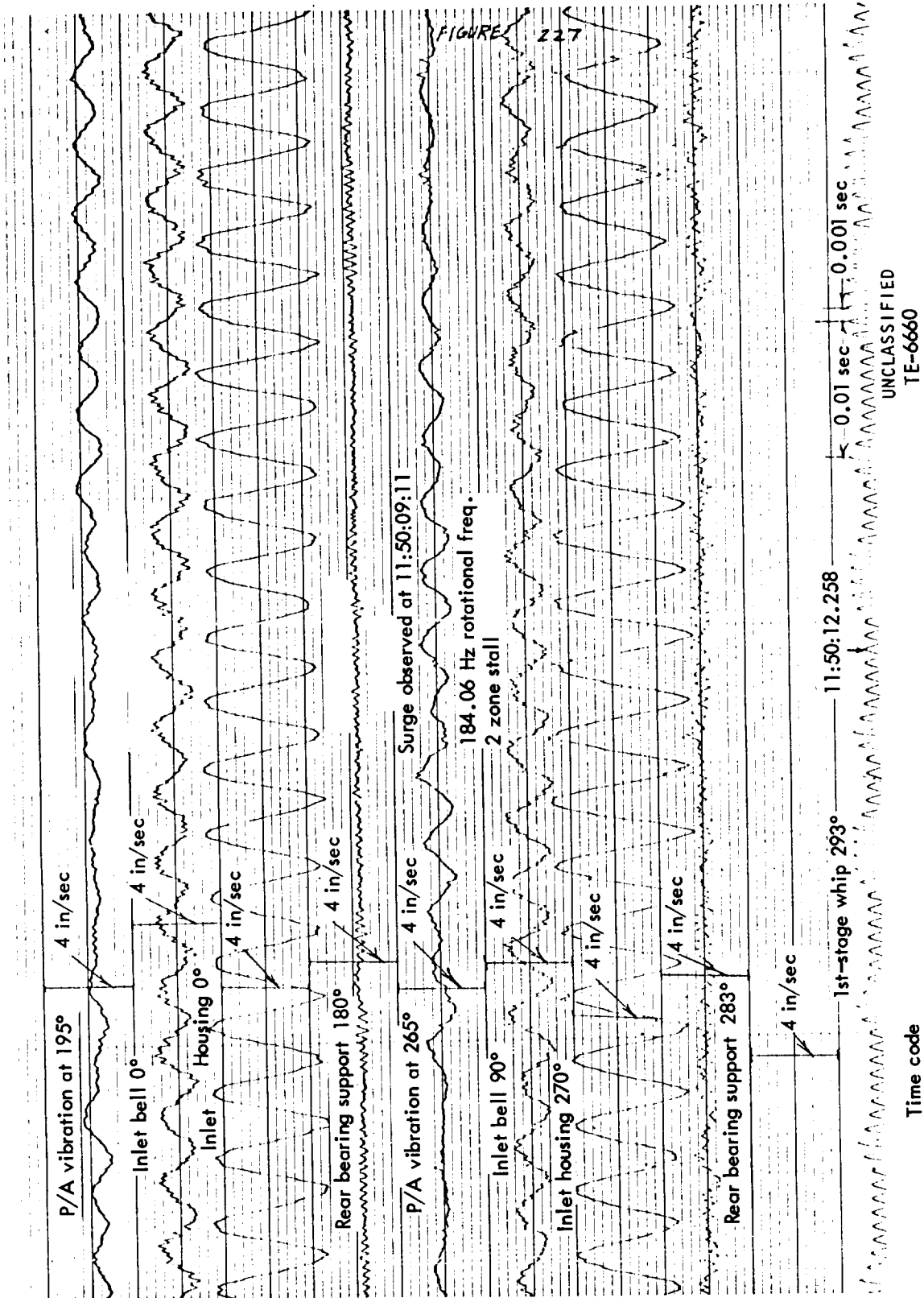Figure 4. - Pressure data during two-zone stall.
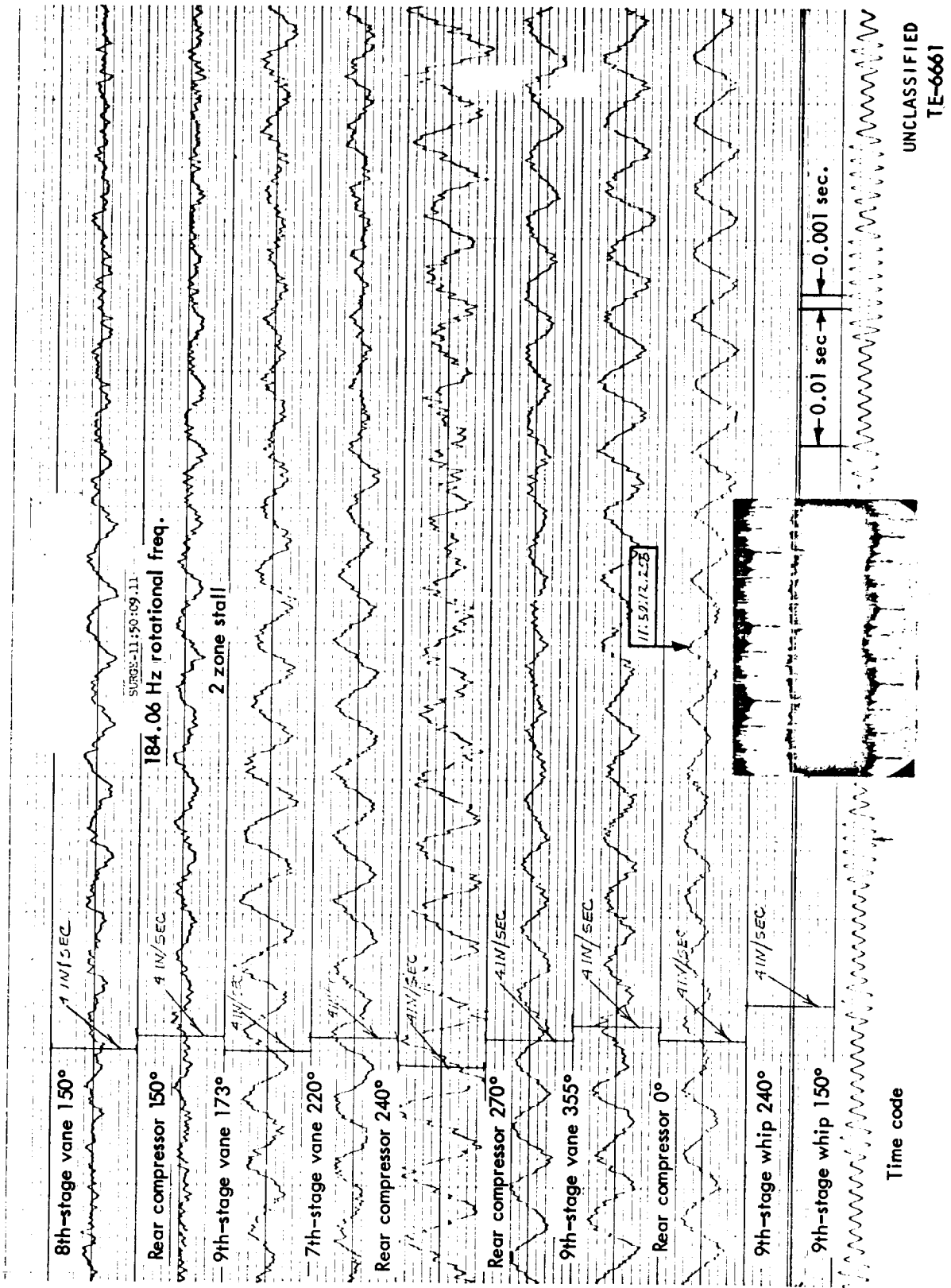
Figure 5. – Vibration induced by two-zone stall.
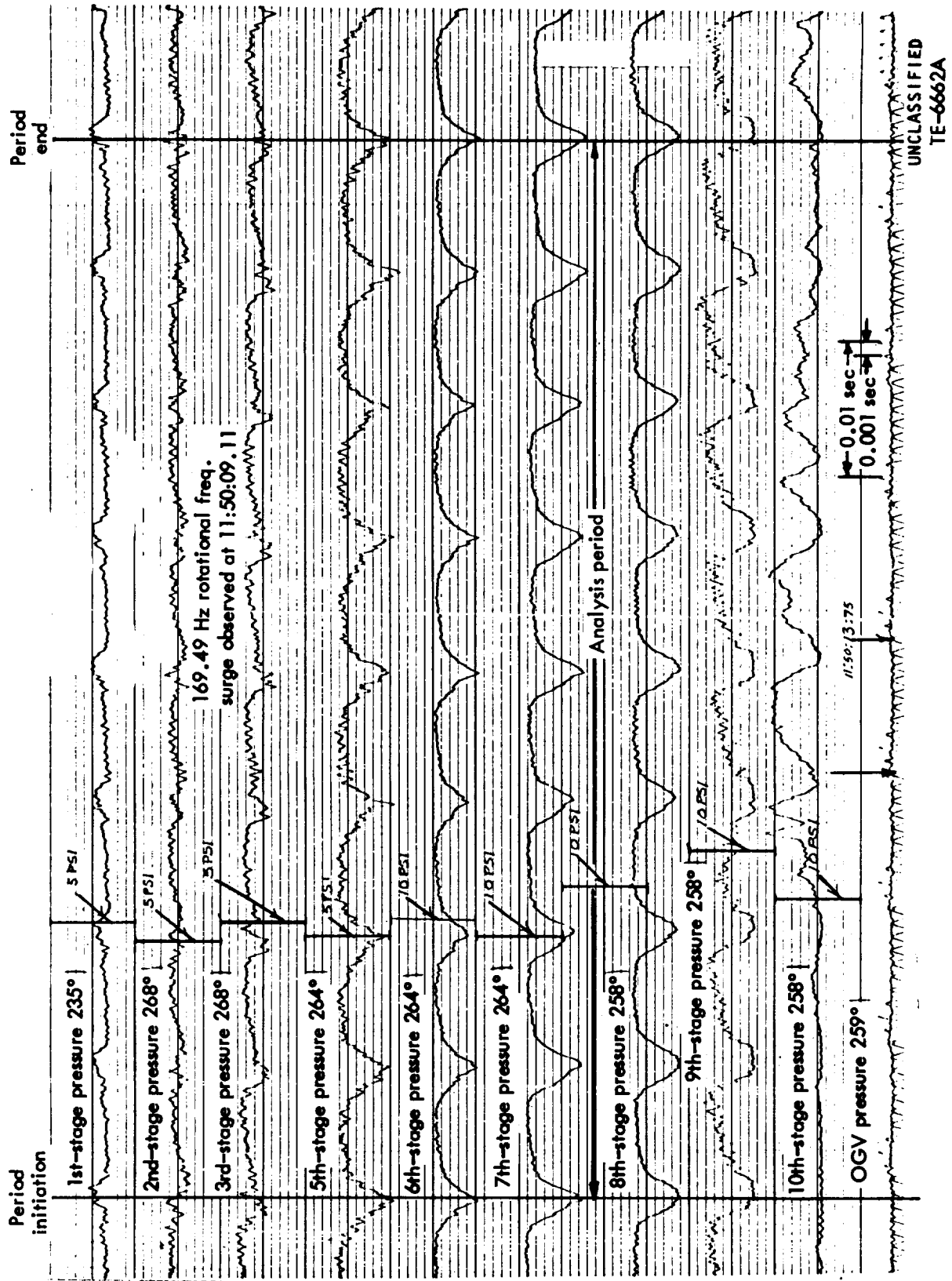
Figure 6. – Vibration induced by two-zone stall.

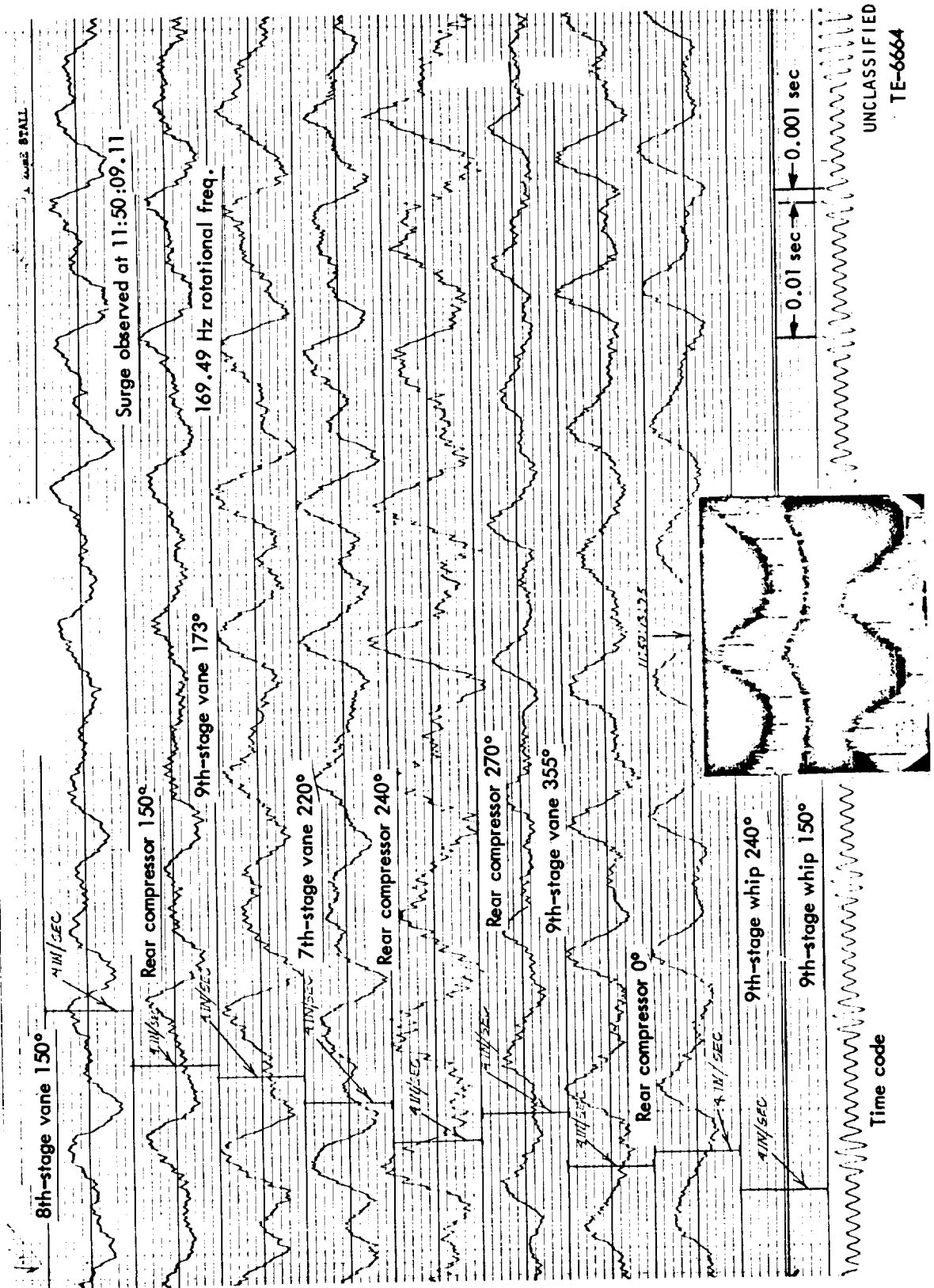Figure 7. – Pressure data during single-zone stall.

411

Figure 8. - Vibration induced by single-zone stall.

TE-6663

412

Figure 9. - Vibration induced by single-zone stall.

413

Beam-like behavior

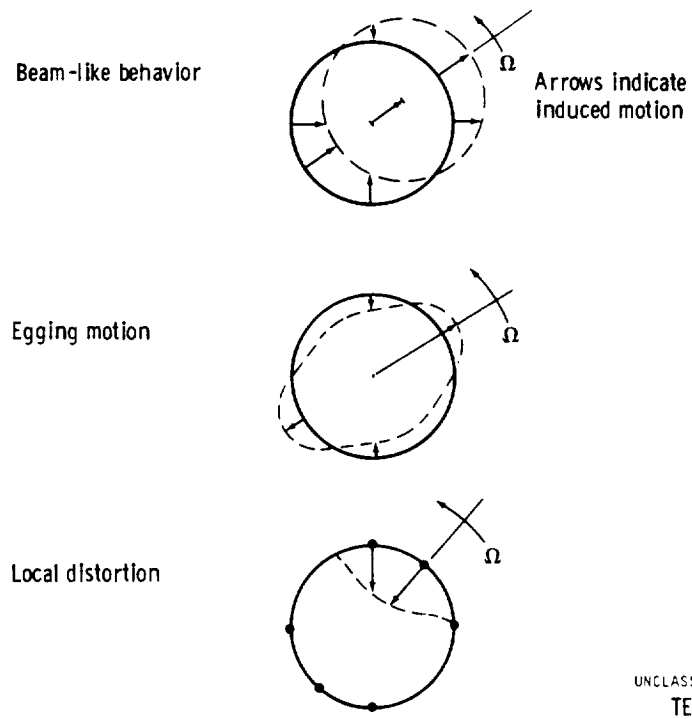Egging motion

Local distortion

Arrows indicate
induced motion

Ω

Ω

Ω

TE-6745

Figure 10. - Case motion descriptions.